JOURNAL OF MATERIALS SCIENCE 32 (1997) 2587–2594

Modelling fracture in laminated architectural glass subject to low velocity impact

F. W. FLOCKER and L. R. DHARANI*
Department of Mechanical and Aerospace Engineering and Engineering Mechanics, University of Missouri-Rolla, Rolla, MO 65409-0050, USA

Standard finite element wave propagation codes are useful for determining stresses caused by colliding bodies; however, their applicability to brittle materials is limited because an accurate treatment of the fracture process is difficult to model. This paper presents a method that allows traditional wave propagation codes to model low velocity, small missile impact in laminated architectural glass such as that which occurs in severe windstorms. Specifically, a method is developed to model typical fractures that occur when laminated glass is impacted by windborne debris. Computational results of concern to architectural glazing designers are presented.

1. Introduction

In this paper we propose a method of modelling fracture due to low velocity, small missile impact of laminated glass windows typically found in large, high-rise buildings. Laminated architectural glazing, as in the familiar automative "safety glass", is constructed by placing an adhesive polymeric interlayer between two soda-lime glass plies. Polyvinyl butyral (PVB) is the industry standard interlayer because of its adhesive and optical qualities. The purpose of the interlayer is to prevent the glass plies from shattering on impact, thereby greatly reducing the possibility of injury caused by sharp pieces of flying glass. In automotive windshield applications, the interlayer also prevents serious passenger injury in a collision by minimizing the possibility of the head penetrating the windshield, and doing so without fracturing the skull. Penetration is prevented by absorbing the impact energy through stretching the PVB interlayer and skull fracture is prevented by reducing the thickness of the glass plies [1]. As will be seen later, the design objectives of architectural glazing are different from automotive glazing in spite of similar construction.

In architectural applications, we are usually concerned with windborne debris such as roof gravel which can be hurled with sufficient velocity to break windows. Beason and co-workers [2] did a study of damage to window glass in Houston, Texas caused by hurricane Alicia which struck Houston in 1983. In that study, significant window damage was reported for a localized area of downtown Houston. The primary cause of window damage was windborne roof gravel. Because Alicia was a relatively mild hurricane, the need for improved impact resistance was apparent in order to be better prepared for the possibility of even stronger hurricanes that may strike.

In their work, Beason and co-workers [2] reported that the outside ply of a laminated unit can serve as an impact shield. Their design methodology allows the outside ply to fracture, but not the inside ply. If the inside ply also fractures, window strength is significantly reduced to the point where wind and/or heating, ventilating and air conditioning loads can cause rapid collapse of the window. This would expose the building interior to the outside weather, greatly increasing the possibility of damage to the building contents, injury to people, and disruption of normal business activity. An impact resistant design that fractures only at the outer ply preserves building envelope integrity and can be replaced at the convenience of the building owner with minimal disruption of occupant activities. It should be noted that this sacrificial ply concept requires that the inside ply itself be of sufficient strength to withstand design wind loading. It is apparent that the design objectives of architectural and automotive glazing are quite different: architectural glazing requires that the inside ply remain intact when subject to low velocity, small missile impact while automotive applications require that both plies fracture when subjected to impact by a vehicle occupant.

The main objective of this work is to present a method whereby traditional finite element wave codes can be used to model low velocity, small missile impact in laminated architectural glass when fracture must be included in the analysis. In addition, results showing the effect of fracture on critical stresses in the laminate are presented.

2. Formulation of the impact problem

Fig. 1 shows the idealized impact problem under consideration. A typical three-layer glazing system is

*Author to whom correspondence should be addressed.

0022–2461

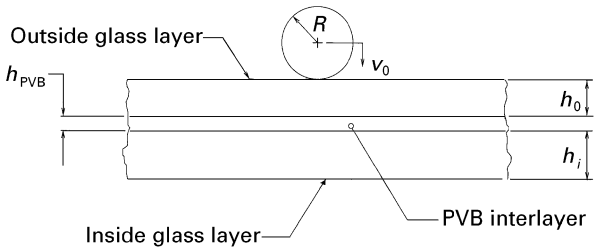

Figure 1 Sketch of the problem studied: glass/PVB/glass laminate subjected to impact by a spherical ball.

considered: two soda-lime glass plies separated by a PVB interlayer. The interlayer bond is assumed perfect with no debonding or slipping between layers during impact. The effect of interlayer delamination will be considered in a future work. The system is impacted by a hard missile modelled as a chromium steel ball with initial impact velocity v_0. A worst-case scenario to simulate windborne roof gravel during a hurricane is assumed: the normal impact of a 7.94 mm diameter steel ball at 35.8 m s^{-1}.

Cylindrical coordinates (r, θ, z) with a Lagrangian description of motion are used to formulate the problem. We assume a condition of torsionless axisymmetry so that normal stresses are independent of the angle θ and the shear stress components $\tau_{r\theta}$ and $\tau_{z\theta}$ vanish. The impact problem is solved numerically using a modified version of the large-scale explicit finite element code DYNA2D [3]. The code was modified to incorporate a cracking algorithm suitable for the impact problem considered here.

The steel ball and inside glass ply are modelled as linear elastic materials. The outside glass ply is modelled as linear elastic with a cracking algorithm detailed below. The PVB interlayer is viscoelastic and is modelled as a so-called standard linear solid. Many polymers follow this linear viscoelastic law very well especially when strains are small [4] as in the case of laminated glass subject to low velocity impact. Details of the material models as well as determination of the various material properties are presented in a previous work [5].

3. Crack systems in glass under impact loading

The main types of cracks that form during the impact of a spherical projectile on a flat brittle surface are cone, median, lateral and radial cracks [6]. Cook and Pharr [7] provide an excellent description of the morphology of each of these crack types. In general, cone and median cracks form during the loading half of the impact cycle while radial and lateral cracks form on unloading. There are of course exceptions; for example, Chaudhri and Walley [8] noted that radial cracks sometimes form just prior to maximum load. At any rate, radial and lateral cracks are generally much shallower than cone and median cracks, are not axisymmetric, and since they usually form after the maximum load has been transmitted to the target (i.e. after the projectile comes to rest and begins to rebound), they have little effect on the maximum stress transmitted through a laminated glass unit to the critical inside ply. Radial and lateral cracks will not be considered in this analysis.

The median crack is also not axisymmetric. It is coin shaped and oriented perpendicular to the target surface directly beneath the impact site. Many researchers [6, 9, 10] believe that median cracks that develop under spherical indenters are due to the formation of a plastic zone of yielded target material beneath the indenter. Although glass is usually considered a brittle material with little or no plastic strain prior to fracture, Marsh [11, 12] showed that plastic flow can occur in glass when the flow stress (von Mises stress) is high enough. Marsh [12] reported that the room temperature flow stress is loading rate dependent and that for short-term, high rate loading, such as found in impact situation, the flow stress in soda-lime glass approaches 10 GPa. We can approximate the maximum von Mises stress occurring during an impact by invoking the so-called quasi-static approximation [13]. That is, stresses occurring during an impact can be well approximated by stresses induced from an equivalent quasi-static load as long as the radius of the contact circle between the colliding bodies expands at a rate below the speed of elastic wave propagation. As shown in the appendix, this is the case for the low velocity impact studied here. Knight, Swain and Chaudhri [6] provide a relation for the maximum equivalent static load, P_{max}, occurring during an impact

$$P_{max} = \left(\frac{125\pi^3 E_t^2 \rho_p^3 v_0^6}{48k^2}\right)^{1/5} R^2 \quad (1)$$

where E denotes Young's modulus, ρ the mass density, v_0 the projectile impact velocity and R the projectile radius. Here and in what follows, the subscripts t and p are used to denote the target and projectile, respectively. The symbol k is used to denote

$$k = \frac{9}{16}[(1-\nu_t^2) + (1-\nu_p^2)(E_t/E_p)] \quad (2)$$

where ν is Poisson's ratio. Using classical Hertz impact theory [14], one can show that the target von Mises stress, $\bar{\sigma}$, at maximum equivalent static load is

$$\bar{\sigma} = p_0\left\{(1+\nu_t)\left[\xi\tan^{-1}\left(\frac{1}{\xi}\right) - 1\right] + \frac{3}{2}\left(\frac{1}{\xi^2+1}\right)\right\} \quad (3)$$

The non-dimensional distance ξ is defined to be z/a where z is the distance into the target from the impact site, p_0 is the maximum interface pressure given by

$$p_0 = \frac{3P_{max}}{2\pi a^2} \quad (4)$$

and a is the maximum contact patch radius during impact given by

$$a^3 = \frac{4kP_{max}R}{3E_t} \quad (5)$$

Differentiating Equation 3 with respect to ξ and setting this equal to zero yields an equation that can be solved numerically to give the location of maximum von Mises stress. This location can then be substituted into Equation 3 to give the maximum von Mises stress during an impact

$$\bar{\sigma}_{max} = \bar{\sigma}|_{\xi=0.4643} = 0.6434 p_0 \quad (6)$$

which is valid for soda-lime glass (i.e. for $\nu_t = 0.25$). Finally, using Equations 1, 4 and 5 in Equation 6 yields

$$\bar{\sigma}_{max} = 0.3398 k^{-4/5} E_t^{4/5} \rho_p^{1/5} v_0^{2/5} \quad (7)$$

where we note that $\bar{\sigma}_{max}$ is independent of the projectile radius. For a steel on glass impact ($E_t = 70$ GPa, $E_p = 200$ GPa, $\nu_t = 0.25$, $\nu_p = 0.29$, $\rho_p = 7800\ kg\,m^{-3}$) at $v_0 = 35.8\ m\,s^{-1}$, Equation 7 yields $\bar{\sigma}_{max} = 5.3$ GPa, well below the flow stress given by Marsh [12] for soda-lime glass at high loading rates. Thus, without plastic flow, we do not expect median cracks to form under the low velocity impact situation studied here. Although the above applies only to the impact of a sphere into an infinite half-space, we will show later that the von Mises stress in a laminated glass unit of finite thickness is less than that in an infinite half-space. Because the von Mises stress is below that required for plastic flow and since plastic flow is the probable cause of median cracks, we conclude that median cracks will not be of concern in the situation studied here. It is also noted that this was the case reported by Ball and McKenzie [15] who saw no evidence of median cracks forming in glass plates under the impact of a steel ball at the velocity considered here.

It is clear from the above that the crack type of primary concern is the cone crack. The cone crack is axisymmetric and originates at the impact surface just outside the contact patch where tensile stresses are the highest. Fig. 2a illustrates a typical cone crack and its geometry. The reason that the cone crack is of primary concern is illustrated in Fig. 2b. The axisymmetric nature of the crack permits a plug to form that can be driven against the PVB interlayer, enhancing delamination. Whether this is harmful or beneficial will be addressed in a future work on interlayer delamination. Of concern here is an accurate model of the cone crack phenomenon and how it affects critical stresses.

4. The computational cone crack model

A propagating cone crack is modelled in a finite element mesh as follows: at the appropriate time and location, an element "cracks" by setting deviatoric stresses and hydrostatic tension to zero. If, in subsequent time steps, deviatoric stresses are computed to be other than zero, they are reset to zero. Similarly, if hydrostatic tension is computed, it is reset to zero. Hydrostatic compression is unaffected in a cracked element. Thus, a cracked element will not support shear or tension but will support compression. A combination of analysis and experimental results detailed below is used to determine the appropriate time and location for element cracking.

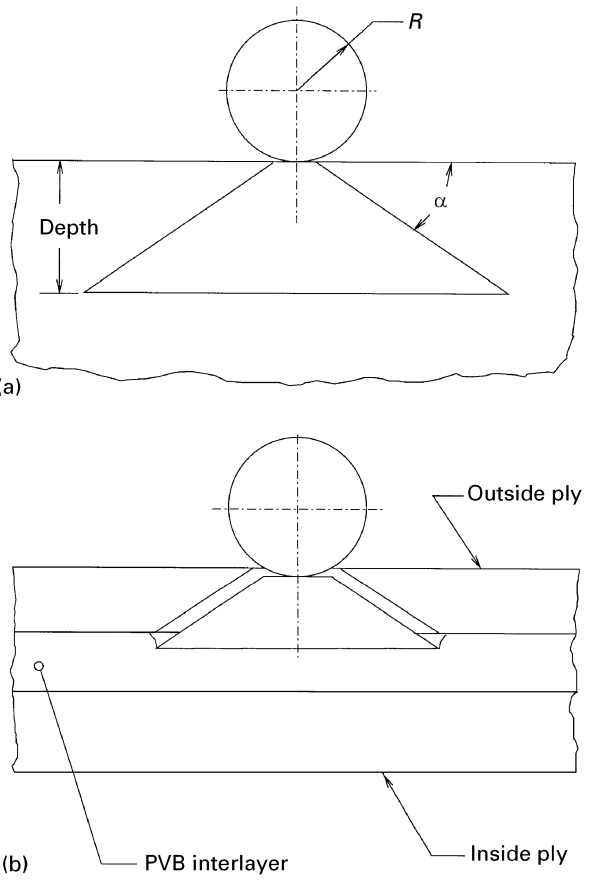

Figure 2 (a) Cone crack and geometry in an infinite half-space; (b) penetrating cone crack in laminated glass unit.

4.1. The crack path

In accordance with experimental observation for impact cases, the cone crack is assumed to originate at the element coinciding with the maximum contact patch radius as given by Equation 5. The cone propagates at an angle α from the surface (see Fig. 2a) where α is a function of impact velocity, v_0. In general, the cone angle increases with increasing impact velocity. The following relation between α and v_0 can be deduced from the experimental work of Knight and colleagues [6] in which 1.0 and 0.8 mm diameter steel balls impacted borosilicate glass. For v_0 less than $50\ m\,s^{-1}$

$$\alpha = \frac{v_0}{290}(90 - \alpha_{st}) + \alpha_{st} \quad (8)$$

where α_{st} is the cone angle for static loading. In the above, both α and α_{st} are in degrees and v_0 is in $m\,s^{-1}$. If we assume the above is also valid for our situation ($R = 3.97$ mm, $v_0 = 35.8\ m\,s^{-1}$) but note that for soda-lime glass, $\alpha_{st} \approx 22^\circ$ [17], we get $\alpha = 30^\circ$.

4.2. Crack velocity

A common approach to describing the velocity of a propagating crack, v_c, is to assume $v_c = [1 - (c_0/c)]v_{max}$ where c_0 is the initial crack length, c is the current crack length and v_{max} is the limiting crack speed [18]. It is easy to show that for the situation here where c is of the order of millimetres and c_0 of the order of micrometres [19] that the assumption

$v_c = v_{max}$ = constant is justified. Experimental observation [8, 18] provides $v_c = 1550\ m\,s^{-1}$.

4.3. Crack initiation time

We now consider when it is appropriate to start cone crack propagation. First we need to determine an approximate relation between equivalent static load, P, and time, t. In the spirit of Goldsmith [20] and Greszczuk [21] we assume

$$P(t) = P_{max}\left[\sin\left(\frac{\pi t}{t_i}\right)\right]^n \quad (9)$$

where P_{max} is given by Equation 1, t_i is the duration of impact and n is a constant to be determined. The duration of impact for an elastic collision of a sphere on a flat surface is given by [22]

$$t_i = \frac{4\sqrt{\pi}R}{5}\frac{\Gamma(2/5)}{\Gamma(9/10)}\left(\frac{400\pi^2k^2\rho_p^2}{81v_0E_t^2}\right)^{1/5} \quad (10)$$

where Γ denotes the gamma function. The exponent n in Equation 9 is determined by requiring that the linear impulse exerted on the projectile from the instant of contact to the instant that the projectile comes to rest ($t_i/2$) be equal to the linear momentum of the projectile at the instant of contact. That is

$$\int_0^{t_i/2} P(t)\,dt = mv_0 \quad (11)$$

where m is the projectile mass. Using Equations 9 and 10, the integral in Equation 11 can be evaluated and simplified further using Equation 1 to yield

$$\Gamma\left(\frac{n+1}{2}\right)\Big/\left[\Gamma\left(\frac{n}{2}+1\right)\right] = \frac{2\Gamma(9/10)}{\Gamma(2/5)} \quad (12)$$

which can be solved numerically to give $n = 1.60$. In comparing the present result with that of Goldman [20] and Greszczuk [21] we note that of the three, the present result is the only one that satisfies the three theoretical requirements of maximum load, impact time and linear impulse.

Before the cone crack propagates downward, a shallow ring crack must completely encircle the contact patch [23]. The critical load to initiate a ring crack is given by one of two relations [24]

$$P_c = \frac{\gamma^{3/2}k^2R^2}{X(\nu_t)E_t^{1/2}c_0^{3/2}} \quad c_0 \ll 0.01a_c \quad (13a)$$

$$P_c = AR \quad c_0 \gtrsim 0.01a_c \quad (13b)$$

The first equation applies to the case where initial pre-existing flaws, c_0, are very small in relation to a_c, the contact radius corresponding to P_c. Here $\gamma(=3.9\ J\,m^{-2})$ is the fracture surface energy [24] and $X(\nu) = \{(3/4)[3(1-\nu^2)(1-2\nu)^2/32\pi]^3\}^{1/2}$. The second equation is the so-called Auerbach law. This law represents the minimum value of P_c and applies when preexisting flaws are large in comparison to the first case. Here $A(=109\,000\ N\,m^{-1})$ is the Auerbach constant [25]. Note that for the Auerbach law, the crack initiation load is independent of flaw size. To determine which equation applies requires knowledge of the flaw distribution in the glass. We assume initially that the Auerbach law holds giving $P_c = 433\ N$ for our case. Then, from Equation 5 with $P_{max} = P_c$ we get $a_c = 0.3$ mm. For the Auerbach law to apply we must have sufficient flaws present that are 3 μm or larger. From Santhanam and Shaw [19], we see that this is the case for "as delivered" soda-lime glass rods. We therefore accept that the Auerbach law holds in this case. Actually, for this case, it can be shown that for flaws down to about 1 μm, there is no difference between the crack initiation load predicted by the two equations (keeping in mind that the Auerbach load represents the minimum value of P_c). From Equation 9, the time corresponding to $P_c = 433\ N$ is 0.6 μs; however, recalling that the cone crack will not propagate downwards until the ring crack has completely encircled the contact patch, cone cracking will certainly start later than 0.6 μs. During a rapidly increasing load, such as in impact, it is probable that ring cracks will spontaneously develop at numerous sites, meaning that the time required to encircle the contact patch will be short. For example, at 1.5 μs, Equation 9 predicts an equivalent load of about 3000 N which by Equation 13a is strong enough to initiate ring cracks at flaw sizes below the practical limit observed in soda-lime glass. Thus, we can say with confidence that the cone crack begins to propagate sometime between 0.6 μs and 1.5 μs after impact. This would be consistent with the experimental results of Chaudhri and Liangyi [26] in which high speed photographs of a tungsten carbide sphere impacting soda-lime glass show the cone crack initiating after the predicted time of initial ring crack formation but still early in the impact cycle. To determine the effect of the uncertainty in cone crack initiation time, two cases were computed: one at an initiation time of 0.6 μs, another at 1.5 μs. The difference between the two computed solutions, for stresses of concern, was negligible. Cone crack initiation times of both 0.6 μs and 1.5 μs were used in the computations that follow.

4.4. Crack depth

The final step is to determine how far the cone crack will propagate. Wiederhorn and Lawn [27] show that for the impact of a sphere on a glass block, the geometry of a cone crack (Fig. 2a) is proportional to $R^{4/3}$ when the same materials and velocity are involved. Therefore, by scaling the experimental data of Ball and McKenzie [15] in which a 5.0 mm diameter steel ball impacted glass plates, it can be shown that for the worst case scenario considered here ($2R = 7.94$ mm, $v_0 = 35.8\ m\,s^{-1}$) that a cone crack can be expected to completely penetrate an 18 mm thick glass plate. Typical architectural glazing uses plies around 5 mm thick; therefore, since 18 mm exceeds the practical ply thickness of architectural glazing, here we will assume that the cone crack completely penetrates the outside glass ply.

5. Finite element computations

We consider the geometry of a typical architectural glazing unit: $h_0 = 4.76$ mm, $h_{PVB} = 1.59$ mm,

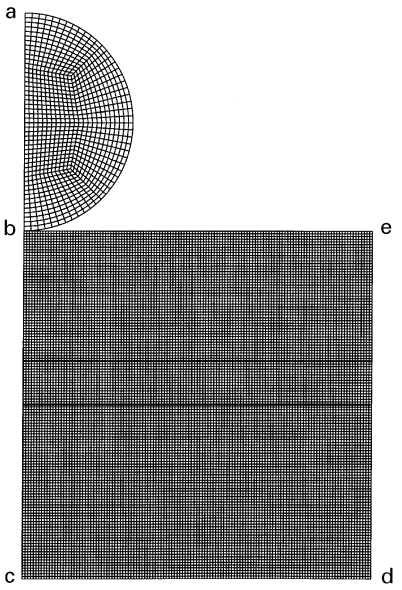

Figure 3 Finite element mesh for the problem studied.

$h_i = 6.35$ mm (see Fig. 1). Fig. 3 shows the finite element mesh which, because of the problem axisymmetry, represents only half of the actual geometry. The bold lines in the figure are used to show the three layers of the laminate. The mesh shown (17 554 nodes) represents the hardware limitation of the machine used in the computations. With regard to numerical convergence, mesh refinement studies without cracking showed a coarser mesh (4643 nodes) to be satisfactory; however, to simulate an actual cracking process, elements need to be kept as small as possible to minimize the strain energy released in cracked elements. There is certainly a violation of the Griffith energy balance requirement here, but small elements will mitigate this effect. In the figure, boundaries c–d and b–e are unconstrained. Boundary d–e is a so-called non-reflecting boundary that is achieved by producing an impedance matching function that cancels incoming stress waves so that none are reflected back from the boundary. Non-reflecting boundaries are used to simulate infinite bodies; in this case, an infinite laminate of finite thickness.

We are concerned mainly with stresses at the surfaces of the glass plies since this is where cracks tend to open and extend under tensile loading [6, 8, 23, 28]. Furthermore, using the design methodology of Beason *et al.* [2], we restrict our concern to surface stresses in the inside glass ply since this is the ply that must not fracture. As shown in a previous work [5], the r, θ and z directions are principal directions for normal impact and furthermore, the radial and hoop stresses are equal and much larger than the axial stress. Therefore, the maximum principal tensile stress is of primary concern since it corresponds to a mode I, crack opening stress for a surface crack located normal to the surface. Following each impact simulation, a search of the maximum tensile principal stress in all elements of the inside ply was done. In each case, the maximum principal tensile stress occurred at element 1 of the mesh located at the innermost surface along the line of symmetry (point c in Fig. 3). Therefore, we are interested in what effect the cone crack has on element 1 maximum tensile principal stresses.

In all computations in this study, the glass plies are considered to be initially free of residual stresses due to thermal treatment; that is, we are considering annealed glass only. Thermally treated glass will be considered in future studies.

6. Results

Fig. 4 shows the cracked elements in relation to the problem geometry. The elements began cracking at the contact path radius at 1.5 μs and propagated downward at 1550 m s^{-1}, reaching the final configuration shown at about 6.1 μs after crack initiation.

Fig. 5 shows the von Mises stresses along the impact load line. Each point on the graph represents the maximum value occurring during an impact cycle. We see that the effect of a cone crack in a laminated glass unit is a lower von Mises stress than that observed when no cracking occurs. Also shown is the case of a theoretical impact of a steel sphere into a glass elastic half-space. Recall we showed that for the steel on glass impact case studied here ($v_0 = 35.8$ m s^{-1}, $2R = 7.94$ mm), the von Mises stresses in an elastic half-space were not high enough to produce plastic flow leading to median cracks. Here, we see that the stresses in a laminated glass unit are less than those in a glass half-space with the stresses even less when a cone crack is introduced. This figure supports the assumption that median cracks do not form in the impact case considered here.

Fig. 6 shows the distribution of maximum principal tensile stress (normalized with respect to the maximum no cracking value) for stations along the inside ply. As discussed earlier, the stress is maximum at the location directly below the impact site. The partial cone cracking case shown is one in which the cone crack was allowed to penetrate only 92% of the thickness of the outside ply. We see that the effect of a cone crack is an approximate 28% increase in the critical mode I stress. Fig. 7 is a time history plot of the critical mode I stress for the cone cracking and no cracking cases. Here, the figure is normalized with respect to the maximum no cracking value. We note that the stress pulse is about 20 μs in duration. This figure will prove useful in future works when it will be necessary to consider the amplitude and duration of the pulse in order to predict when a given pulse will open and extend a pre-existing flaw.

One clear consequence of the cone crack formation, evident from Fig. 2b, is the certainty of high stress concentrations at the interface between the cone crack and PVB interlayer. These stresses will play a key role in delaminating the PVB interlayer which will affect the critical inside ply mode I stress. The effect of delamination on critical mode I stress will be studied in a future work; here we simply note that the cone crack provides large stress concentrations that may promote delamination. Figs 8 and 9 are plots of the maximum axial and shear stress occurring along the interface between the outside glass ply and the PVB interlayer, respectively. The distance along the

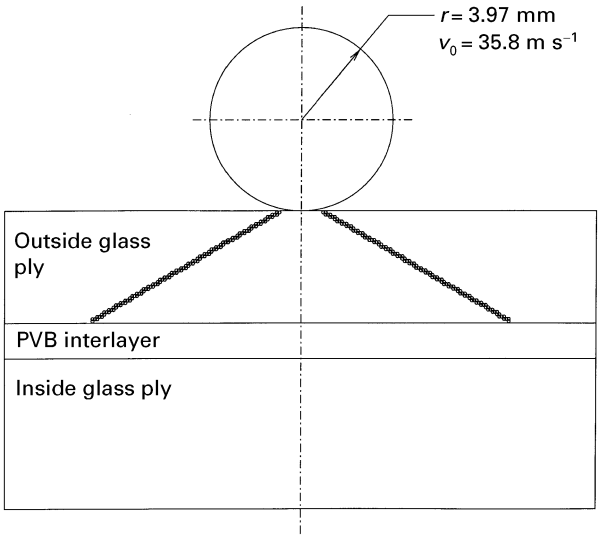

Figure 4 Illustration of cracked elements following impact.

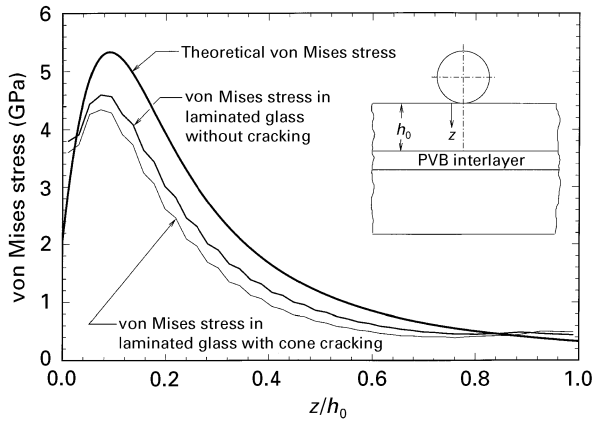

Figure 5 von Mises stresses in the outside ply along the impact load line.

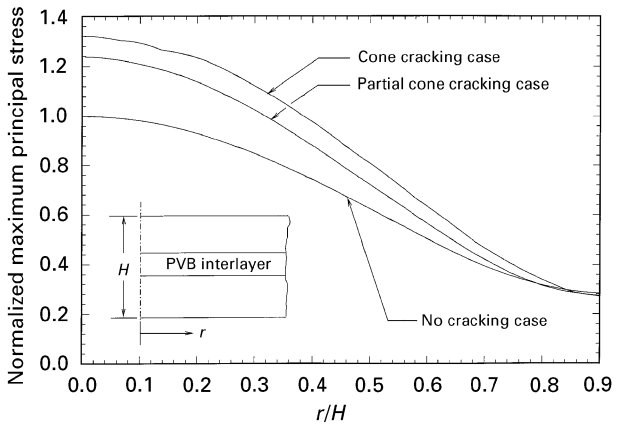

Figure 6 Normalized maximum principal stress along the inside surface of the laminate.

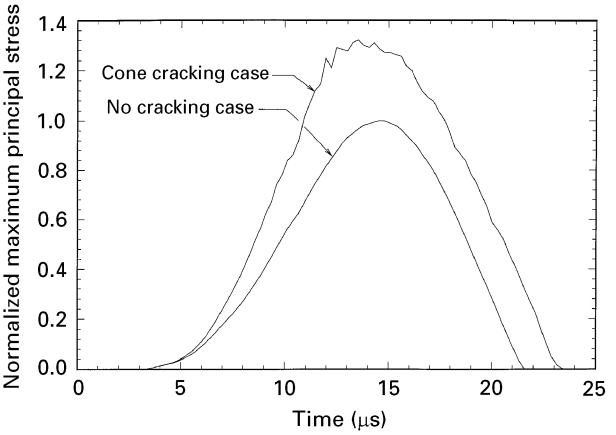

Figure 7 Normalized maximum principal stress as a function of time for the critical element.

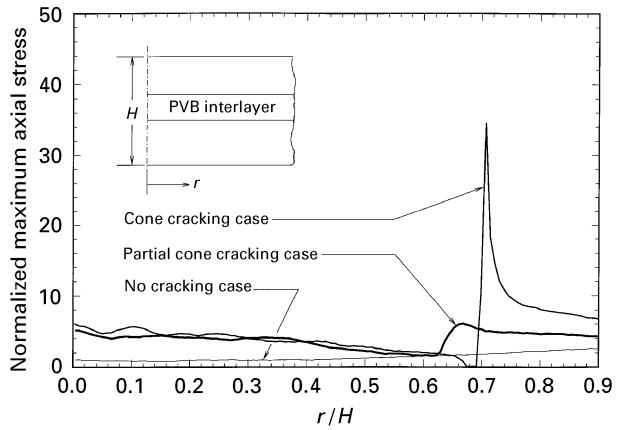

Figure 8 Normalized maximum axial stress along the outside ply/PVB interface.

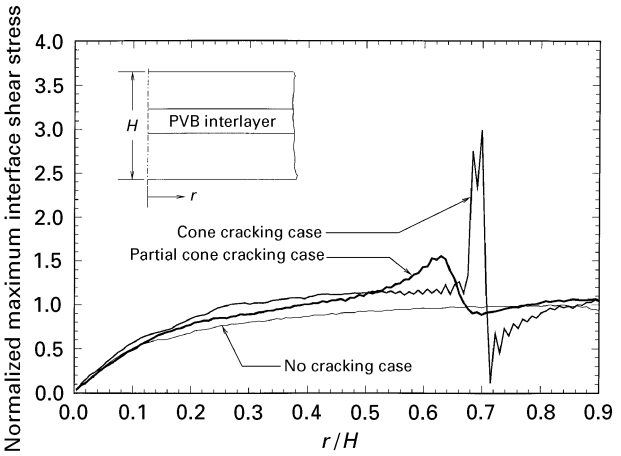

Figure 9 Normalized maximum shear stress along the outside ply/PVB interface.

interface, r, is normalized with respect to the overall laminate thickness, H. The axial stress is normalized with respect to the no cracking case at $r = 0$, while the shear stress is normalized with respect to the maximum value for the no cracking case. From both figures, we note the high stress levels where the cone crack meets the PVB interlayer and also note the dramatic mitigation of the stress concentration for the partial cone cracking case (crack penetrates 92% of the outside ply thickness).

We now consider the effect of a cone crack when there is a mechanism for providing the transfer of force between the plug formed by the cone crack and the remainder of the glass ply. Such a mechanism might be provided by a second phase of tough whiskers, particles of fibres that could bridge the cone crack in

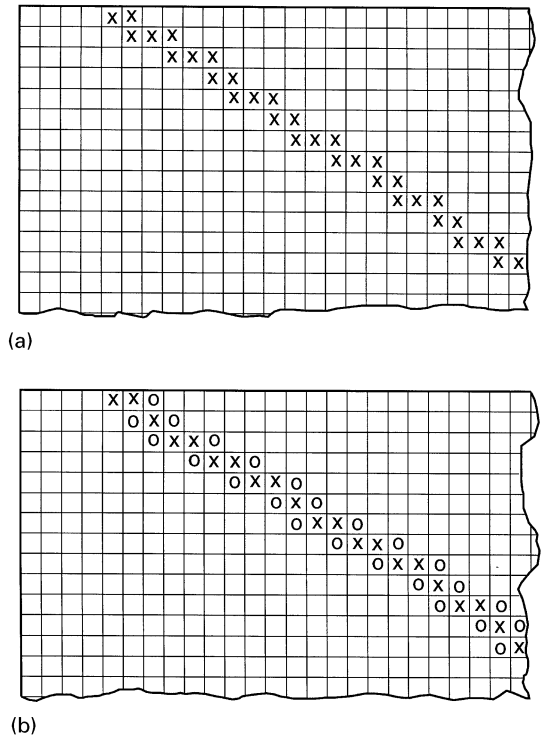

Figure 10 Cracked element pattern. (a) No mechanical interlocking; (b) with mechanical interlocking.

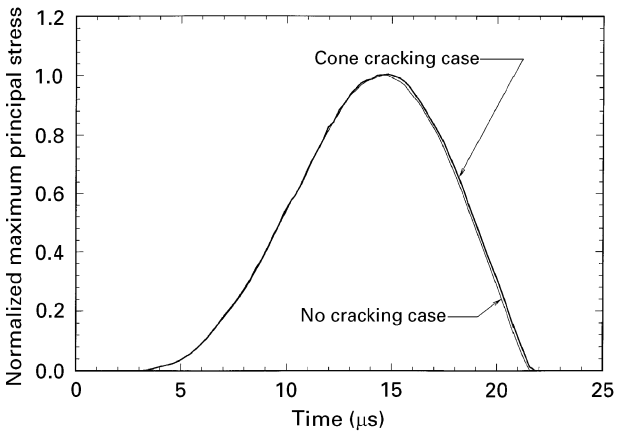

Figure 11 Normalized maximum principal stress as a function of time for the critical element with mechanical interlocking across the cone crack face.

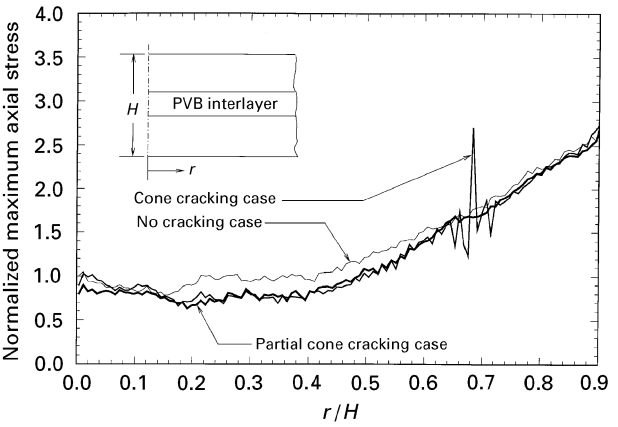

Figure 12 Normalized maximum axial stress along the outside ply/PVB interface with mechanical interlocking across the cone crack face.

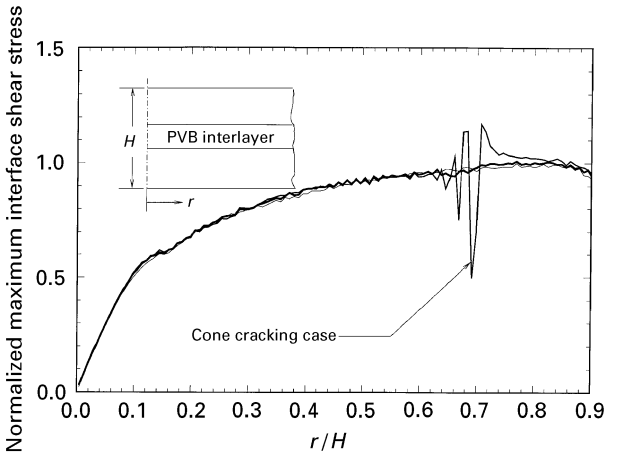

Figure 13 Normalized maximum shear stress along the outside ply/PVB interface with mechanical interlocking across the cone crack face.

much the same way that crack bridging occurs in successful reinforced brittle matrix composites (clearly, this would provide a substantial challenge to the materials designer in order that optical qualities are not sacrificed). The modelling of a force transfer mechanism is achieved in a qualitative fashion by modifying the cracking algorithm employed earlier. Fig. 10a is a schematic of the cracked mesh used previously, an "x" denoting a cracked element. Recalling the definition of a cracked element, it is evident from the schematic that tensile force cannot be transferred across the crack. Fig. 10b is a schematic of a mesh in which tensile force transfer between certain elements is allowed. Cracked elements are those marked with an "x". For this mesh, forces can interact through the nodes between elements marked with an "o". Figs 11, 12 and 13 show the effect of mechanical interlocking on the mode I stress and the interface axial and shear stresses, respectively. We note the significant reduction (c.f. Figs 7, 8, 9) of all critical stresses when mechanical interlocking is provided.

7. Conclusions

This work proposes an effective method in which traditional finite element wave codes can be used to analyse low velocity, small missile impact damage in laminated architectural glazing. The work provides much of the analytical and computation framework for the future development of a computational model that can be used to predict inside ply fracture in architectural glazing systems due to windborne debris impact.

It was shown that the primary crack type of concern to the laminated architectural glass designer with regard to impact resistance is the Hertz cone crack. The cone crack was shown to completely penetrate the outside ply of a three-layer system for practical

applications when subjected to the worst-case scenario occurring in severe windstorms.

Arresting the cone crack before complete penetration was shown to result in a reduction in all critical stress measures; however, it remains to be seen in future works what effect interlayer delamination plies in the critical mode I stress in the inside ply. In addition, the qualitative effect of mechanical interlocking between the regions separated by the cone crack was shown to be a significant reduction in critical stresses.

Appendix: Rate of contact circle expansion during impact

The assumption that stresses due to an elastic impact are well approximated by the stresses caused by an equivalent quasi-static load is valid as long as the contact circle between the projectile and target expands at a rate less than the velocity of elastic waves in the target [13]. To determine the rate at which the contact radius expands during impact, we rewrite Equation 5 so that the contact radius is a function of time

$$a(t) = \left(\frac{4kP(t)R}{3E_t}\right)^{1/3} \quad \text{(A1)}$$

Substituting Equation 9 into Equation (A1) and differentiating with respect to time gives the rate of contact radius expansion

$$\dot{a}(t) = \frac{n\pi}{3t_i}\left(\frac{4kRP_{max}}{3E_t}\right)^{1/3}\left[\sin\left(\frac{\pi t}{t_i}\right)\right]^{\frac{n-3}{3}}\cos\left(\frac{\pi t}{t_i}\right) \quad \text{(A2)}$$

where P_{max} is given by Equation 1, t_i by Equation 10 and $n = 1.6$. Equation (A2) is plotted in Fig. A1 for the case of a steel-on-glass impact ($E_t = 70$ GPa, $E_p = 200$ GPa, $\nu_t = 0.25$, $\nu_p = 0.29$, $\rho_p = 7800\ \mathrm{kg\,m^{-3}}$) and $v_0 = 35.8\ \mathrm{m\,s^{-1}}$, $R = 3.97$ mm. Note that except for singularities at the moments of impact and leaving, $\dot{a}$ is well below the velocity of stress wave propagation in glass ($\approx 5800\ \mathrm{m\,s^{-1}}$ for dilatational waves, $3100\ \mathrm{m\,s^{-1}}$ for Rayleigh surface waves) and therefore the stresses due to an elastic impact are well approximated by the stresses due to an equivalent quasi-static load.

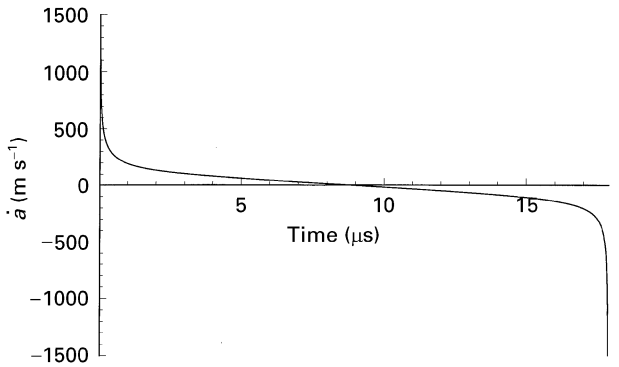

Figure A1 Expansion rate of contact patch radius.

References

1. J. R. HUNTSBERGER, *J. Adhesion* **13** (1981) 107.
2. W. L. BEASON, G. E. MEYERS and R. W. JAMES, *J. Struct. Eng.* **110** (1984) 2843.
3. R. G. WHIRLEY, B. E. ENGLEMANN and J. O. HALQUIST, "DYNA2D, a nonlinear, explicit, two-dimensional finite element code for solid mechanics," User manual, Lawrence Livermore National Laboratory Report, UCRL-MA-110630, 1992.
4. Y. C. FUNG, "Foundations of solid mechanics" (Prentice-Hall, Englewood Cliffs, NJ, 1965) p. 20.
5. F. W. FLOCKER and L. R. DHARANI, *Eng. Struct.* accepted.
6. C. G. KNIGHT, M. V. SWAIN and M. M. CHAUDHRI, *J. Mater. Sci.* **12** (1977) 1573.
7. R. F. COOK and G. M. PHARR, *J. Amer. Ceram. Soc.* **73** (1990) 787.
8. M. M. CHAUDHRI and S. M. WALLEY, *Phil. Mag. A* **37** (1978) 153.
9. M. V. SWAIN and J. T. HAGAN, *J. Phys. D: Appl. Phys.* **9** (1976) 2201.
10. B. LAWN and R. WILSHAW, *J. Mater. Sci.* **10** (1975) 1049.
11. D. M. MARSH, *Proc. Roy. Soc. London, A* **279** (1961) 420.
12. *Idem., ibid.* **282** (1964) 33.
13. S. C. HUNTER, *J. Mech. Phys. Solids* **5** (1957) 162.
14. S. P. TIMOSHENKO and J. N. GOODIER "Theory of elasticity" 3rd edn (McGraw-Hill, New York, 1970) pp. 409–20.
15. A. BALL and H. W. MCKENZIE, *J. de Physique IV* **4** (1994) C8-783.
16. J. PERSON, K. BREDER and D. J. ROWCLIFFE, *J. Mater. Sci.* **28** (1993) 6484.
17. B. R. LAWN, T. R. WILSHAW and N. E. W. HARTLEY, *Int. J. Fract.* **10** (1974) 1.
18. M. F. KANNINEN and C. H. POPELAR "Advanced fracture mechanics" (Oxford University Press, New York, 1985) pp. 409–20.
19. S. SANTHANAM and M. C. SHAW, *J. Amer. Ceram. Soc.* **73** (1990) 2922.
20. W. GOLDSMITH "Impact: The theory and physical behaviour of colliding solids" (Edward Arnold, London, 1960) pp. 82–137.
21. L. B. GRESZCZUK in "Impact dynamics" edited by Z. A. Zukas, T. Nicholas, H. Swift, and L. B. Greszczuk (John Wiley & Sons, New York, 1982) pp. 55–94.
22. A. E. H. LOVE "A treatise on the mathematical theory of elasticity" 4th edn (Dover, New York 1994) p. 198.
23. F. C. FRANK and B. R. LAWN, *Proc. Roy. Soc. London A* **299** (1967) 291.
24. B. R. LAWN and S. M. WIEDERHORN, *J. Amer. Ceram. Soc.* **58** (1975) 428.
25. B. LAWN "Fracture of brittle solids" 2nd edn (Cambridge University Press, New York, 1993) p. 286.
26. M. M. CHAUDHRI and C. LIANGYI, *J. Mater. Sci.* **24** (1989) 3441.
27. S. M. WIEDERHORN and B. R. LAWN, *J. Amer. Ceram. Soc.* **60** (1977) 451.
28. M. M. CHAUDHRI and C. R. KURKJIAN, *ibid.* **69** (1986) 404.

Received 18 June
and accepted 23 October 1996